Twenty-Seventh Symposium (International) on Combustion/The Combustion Institute, 1998/pp. 587–594

INTERACTION OF A VORTEX WITH A FLAT FLAME FORMED BETWEEN OPPOSING JETS OF HYDROGEN AND AIR

V. R. KATTA,[1] C. D. CARTER,[1] G. J. FIECHTNER,[1] W. M. ROQUEMORE,[2] J. R. GORD[2] AND J. C. ROLON[3]

[1]*Innovative Scientific Solutions, Inc.*
2766 Indian Ripple Road
Dayton, OH 45440-3638, USA
[2]*Propulsion Directorate*
Air Force Research Laboratory
Wright-Patterson Air Force Base, OH 45433-7103, USA
[3]*E.M2.C Laboratory, CNRS*
Ecole Centrale Paris
92295 Chatenay-Malabry Cedex, France

Studies on individual vortex-flame interactions constitute important elements for the understanding of the turbulent-flame structure. Vortices having sufficiently high normal velocity can pass through the flame by extinguishing it locally. In several circumstances, they deform the flame surface significantly before attaining extinction conditions. The development of curvature on the flame surface, especially in hydrogen flames, could lead to different quenching patterns. An experimental/numerical investigation is performed to explore possible quenching patterns in opposing-jet diffusion flames. A diluted hydrogen-nitrogen mixture is used as the fuel. Vortices are driven toward the flame surface with different velocities from the air side. The changes in the structure of the flame during its interaction with the incoming vortex are recorded by measuring instantaneous OH-concentration fields using the laser-induced fluorescence (LIF) technique. A time-dependent CFDC code that incorporates 13 species and 74 reactions is used for the simulation of these vortex-flame interactions. Both the experiments and calculations have identified two types of quenching patterns; namely, point and annular. It is found that when an air-side vortex is forced toward the flame at a relatively high speed, then the flame at the stagnation line quenches, resulting in a well-known point-quenching pattern. On the other hand, when the vortex is forced at a moderate speed, the flame surface deforms significantly, and quenching develops in an annular ring away from the stagnation line, resulting in an unusual annular-quenching pattern. Detailed analyses performed just before the development of annular quenching and 1 ms later suggest that this unusual annular quenching did not result from the strain rate. Based on the understanding gained from previous investigations on curvature effects in coaxial hydrogen jet flames and the findings made in the present study, it is argued that such quenching develops as a result of the combined effect of preferential diffusion and flame curvature.

Introduction

Recently, numerous investigations (experimental and numerical) [1–3] have been performed to quantify the scalar structure of steady state, aerodynamically strained, planar diffusion flames. Such studies on counterflow diffusion flames have not only provided benchmark experimental data but also yielded valuable insight into the flame behavior in response to strain rate. However, in practical combustion devices, flames are subjected to severe unsteadiness resulting from the random motion of vortices [4,5]; this has led to studies of unsteady counterflow flames. To retain the simplicity offered by planar diffusion flames, unsteadiness is imposed on counterflow flames by fluctuating the fuel and air jets simultaneously and sinusoidally [6,7]. These studies have demonstrated that the unsteady flames can be stretched beyond the steady-state extinction limit.

During vortex-flame interactions, which are often considered as the building blocks for statistical theories of turbulence, the flame surface is subjected not only to unsteadiness but also to deformation. Studies of Law [8], Mizomoto et al. [9], and Takagi and Xu [10] have shown that the structure of a flamelet depends on the curvature and the preferential diffusion associated with species having different molecular weights. To investigate the effects of curvature on flame structure, both theoretical and experimental studies have been initiated. In particular, experiments designed by Roberts et al. [11] and Rolon [12] have created great interest, especially because of their unique abilities to shoot a well-characterized vortex toward the flame surface.

Several investigators have developed models [13–15] for the study of vortex-flame interactions in opposing-jet flames. In all of these models, it is

assumed that an artificially created vortex pair (by specifying the vorticity field) interacts with a flat flame formed in a parallel flow. Although such an assumption has advantages in exploring interesting aspects of the vortex-flame interactions, these investigations do not represent the actual interactions in opposing-jet flames; hence, they could not yield direct comparisons between predictions and measurements.

Recent advances in computer-hardware technology and the need for improving the understanding of combustion phenomena under complex practical situations have led to the development of two- and three-dimensional computational fluid dynamics models that incorporate detailed chemical kinetics [16,17]. However, to our knowledge, no complete simulation of the counterflow diffusion flame has yet been reported. Such simulations would not only eliminate the concerns of the simplified analyses but also provide a valuable tool for studies of vortex-flame interactions in counterflow premixed [11] and diffusion [12] flames.

This paper describes a numerical and experimental study performed on the vortex-flame interactions in a hydrogen opposing-jet diffusion flame. The Computational Fluid Dynamics with Chemistry (CFDC) code was validated by direct simulation of the steady-state counterflow diffusion flame. The calculated instantaneous flowfield that reveals the annular-quenching pattern is compared with the measured OH-concentration image. The processes leading to annular quenching during the vortex-flame interaction are investigated by analyzing the flame structures obtained at different locations and times.

Mathematical Model

Time-dependent, axisymmetric Navier–Stokes equations written in the cylindrical-coordinate (z-r) system are solved along with species- and energy-conservation equations [18]. A detailed chemical-kinetics model has been used to describe hydrogen-air combustion. This model consists of 13 species; namely, H_2, O_2, H, O, OH, H_2O, HO_2, H_2O_2, N, NO, NO_2, N_2O, and N_2. A detailed chemical-kinetics model having 74 reactions among the constituent species is used, and the rate constants for this H_2-O_2-N_2 reaction system were obtained from Ref. [19].

Temperature- and species-dependent property calculations are incorporated in the model. The enthalpy of each species is calculated from polynomial curve fits that were developed for the temperature range of 300–5000 K. The viscosity and thermal conductivity of individual species are estimated from the Chapman–Enskog collision theory, and the mixture properties are obtained using Wilke's semiempirical formulae. The effective binary-diffusion coefficient of the individual species in the local mixture is calculated using molecular dynamics and the Lennard–Jones potentials.

The governing equations are integrated on a nonuniform staggered-grid system. An orthogonal grid having rapidly expanding cell sizes in both the axial and radial directions is employed. The finite-difference forms of the momentum equations are obtained using an implicit QUICKEST scheme [20,21], and those of the species and energy equations are obtained using a hybrid scheme of upwind and central differencing. At every time step, the pressure field is calculated by solving the pressure Poisson equations simultaneously and utilizing the LU (Lower and Upper diagonal) matrix-decomposition technique.

Experimental Setup

The burner geometry used for the vortex-flame-interaction studies in opposing-jet flames was initially designed by Rolon [12]. It consists of 25-mm-diameter inner nozzles, 40-mm-diameter outer nozzles, and syringe tubes of 5-mm diameter. Fuel (a mixture of hydrogen and nitrogen) and air are fed through the upper- and lower-inner nozzles, respectively. Nitrogen was used in the outer nozzles to shield the flame from the ambient air. Even though the tip of the syringe tube is placed 5 mm upstream of the inner nozzle exit in the experiment, it has been assumed to be flush with the nozzle exit in the present numerical investigations. In a typical experiment, a steady-state opposing-flow jet flame is initially established by flowing fuel and air at specified flow rates through the respective nozzles. Vortices are shot toward the flame surface from either the fuel or the air side by rapidly injecting a specified amount of fluid from the respective syringe tube. The vortices are usually characterized [12] by the amount and duration of fluid injection. The resulting changes in the structure of the flame because of its interaction with the approaching vortex are recorded by measuring instantaneous relative OH-concentration fields using the laser-induced fluorescence (LIF) technique.

Results and Discussion

Experiments were performed using this burner for different flow conditions and vortex sizes and shapes. In the present study, the flat flame formed between the fuel and air jets having velocities of 0.69 and 0.5 m/s, respectively, is considered. The hydrogen-to-nitrogen molar ratio used for the fuel jet is 0.38. Calculations for this axisymmetric flame were made using a nonuniform 301 $\times$ 121 mesh system that yielded a mesh spacing of 0.1 mm in both axial (z) and radial (r) directions in the region of interest.

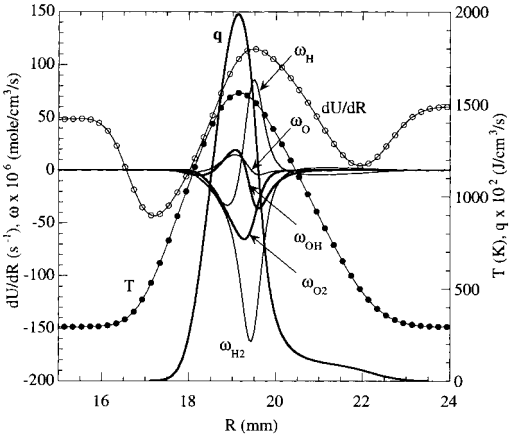

FIG. 1. Structure of steady-state flame established between 37.6% H_2 diluted with N_2 and air jets. Air-side strain rate induced on the flame is 48 s^{-1}.

Steady-State Flame Structure

The CFDC model developed for the simulation of a time-dependent jet diffusion flame was previously validated by simulating the counterflow jet diffusion flames studied by Sung et al. [22] and the coaxial flames investigated by Grisch et al. [23]. The computed flame structure at the stagnation line of the steady-state flame used in this study is shown in Fig. 1 in the form of distributions of velocity gradient normal to the flame (dU/dR), molar production rates of various species (ω_i), temperature (T), and heat release rate (q). Here R represents the line that is normal to the flame surface. Note that since the flame is symmetric, the normal to the flame surface at this location coincides with the stagnation line. The flame structure shown in Fig. 1 is not compared with the experimental one because of the lack of quantitative data; however, it compares well with that of a typical opposing-jet diffusion flame [22]. On the other hand, the calculations made for slightly different flow rates yielded good agreement with the experimental data of Rolon [12].

An opposing-jet flame is usually characterized by the air-side strain rate (K_{air}), which may be obtained by calculating the maximum velocity gradient on the air side of the flame [3]. The 48-s^{-1} strain rate of the steady-state flame in Fig. 1 represents that of a weakly strained flame. In general, the peak strain rate on the fuel side (60 s^{-1}) will be greater than that on the air side as a result of the difference in the density of the two jets. Although the peaks in production rates of O and OH radicals appear on the air side of the flame (peak temperature or heat-release-rate location), the H radicals are produced at the highest rate on the fuel side. Because the flame surface is flat (zero curvature) at this location, the flame structure is not affected by the preferential diffusion of various species having different Lewis numbers in a hydrogen flame.

The steady-state strain rate on the opposing-jet flame can be increased by gradually increasing the velocities of the fuel and air jets. Calculations were repeated by varying jet velocities, and it was found that a stable steady-state flame can be obtained for maximum fuel and air jet velocities of 16 and 14 m/s, respectively. These velocities yielded an air-side strain rate (K_{air}) and flame temperature of 1410 s^{-1} and 1130 K, respectively; these values agree favorably with calculations made by Gutheil et al. [24] using full chemistry for hydrogen-air combustion.

Vortex-Flame Interaction

As discussed earlier, vortices are shot toward the flame surface from the air side by injecting a specified amount of fluid (2.2 cm^3 of air) through the syringe tube. Vortex evolution and its interaction with the flame surface depend on the injection time. In general, with the shorter injection times, the generated vortices travel faster toward the flame surface and affect its structure as the local flow time scales approach the chemical time scales. When the former time scales decrease to a certain level, one might expect localized quenching on the flame surface. On the other hand, the flame surface develops more curvature during the vortex-flame interaction with a slower vortex as the flow time scales become comparable to the diffusion time scales. Because of the preferential diffusion of different species in hydrogen flames, the curvature of the flame can also affect its chemical structure, which means that in hydrogen flames both the faster- and slower-moving vortices could affect the flame structure.

Experiments were conducted on vortex-flame interactions by changing the injection time. Instantaneous flame structures were obtained by recording OH-concentration distributions. As expected, for shorter injection times, the vortex was able to quench the flame at the stagnation line (point quenching) and penetrate through the hole formed on the flame surface. Interestingly, for longer injection times, the vortex deformed the flame surface significantly, and it was observed that quenching on the flame surface first occurs annularly at a location 5-mm radially outward from the stagnation line and then propagates toward the stagnation line ($r = 0$). The OH image obtained for the 10-ms injection-time condition is shown in Fig. 2. This instantaneous image was obtained using the LIF technique. It is known that the concentration of OH in a flame correlates well with the reaction zone. Fig. 2 suggests that the vortex, having a diameter of 13 mm, traveling from the air side has shifted the flame (reaction zone) at the stagnation line by about 0.6 diameter. Note that because the steady-state flame used in this

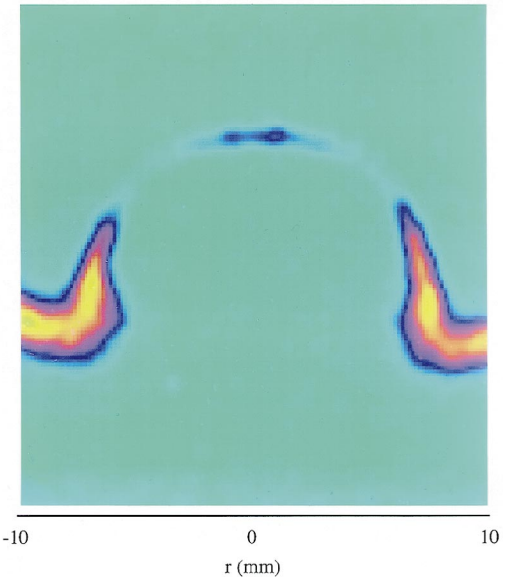

FIG. 2. Relative concentration of OH measured 10 ms after firing the vortex toward the flame. Experiment was performed using the LIF technique.

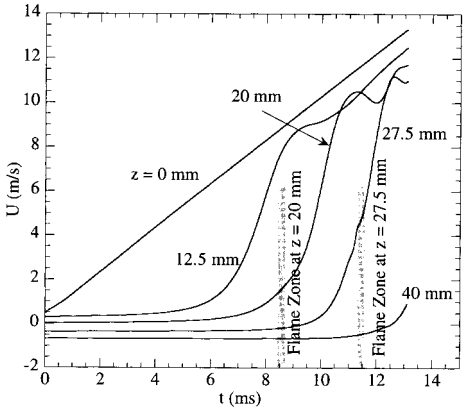

FIG. 3. Variation of local normal velocities with time obtained at four locations along the stagnation line. Straight line with a slope of 10^3 m/s/s at $z = 0$ represents the perturbation velocity imposed at the exit of the air nozzle.

study is a weakly strained one, the OH concentration in the unperturbed flame section (bright yellow) is much higher than that in the highly strained flame zone (dark blue) at the center. Disappearance of OH in the region 4.2 mm $< r <$ 5.2 mm suggests that the flame is quenched. A few milliseconds later the flame in the region $r <$ 5.3 mm is completely extinguished.

The phenomenon of flame extinction in an annular region rather than in the intuitively expected region around the stagnation line could result from either (1) maximum strain rate developing in the region other than at the stagnation line or (2) combined effect of preferential diffusion and flame curvature reducing the reaction rates at a location other than the maximum-strain-rate region. To investigate the role of these possible effects during the vortex-flame interaction shown in Fig. 2, calculations were performed using the time-dependent CFDC code discussed earlier. Flow conditions for the steady-state flame were matched with those used in the experiment, and the computed flame structure is shown in Fig. 1. The unsteady simulations were then performed by injecting air through the central syringe tube in such a way that the velocity at the exit increased linearly at a rate of 10^3 m/s/s.

The axial velocities recorded at four locations along the stagnation line ($z = 0$, 12.5, 20, and 27.5 mm) are plotted with respect to time in Fig. 3. The profile at $z = 0$ represents the one used as the transient boundary conditions for the vortex-flame interaction simulation. At $t = 0$ the flame was located at $z = 19.2$ mm (cf. Fig. 1). In the opposing-flow configuration, the linearly increasing velocity profile transformed into a wave-like profile as the injected mass approached the stagnation point. The times at which the flame surface passed through the axial locations $z = 20$ and 27.5 mm are indicated in Fig. 3 by shaded regions. The increasing velocity in the flame zones (shaded areas) located farther upstream suggests that the separation between the vortex and the flame surface is decreasing with time.

The computed flowfields at four instants (9.1, 11.1, 12.1 and 12.54 ms) during the vortex-flame interaction are shown in Fig. 4. Here, temperature and OH-concentration fields are plotted on the right and left halves, respectively. The instantaneous locations of all the particles that were injected from the air-side nozzles are shown in white, and those injected from the fuel-side nozzles are shown in yellow. Note that the z axis in Figs. 4a to 4d is shifted to accommodate the vortex. A few observations that can be made from these instantaneous plots: (1) the OH zone is thinner than the temperature field and is shifted toward the air side (from which the vortex is coming) of the peak-temperature surface, (2) as the stagnation plane (surface that separates the convective flows from the fuel and air sides) forms on the fuel side of the peak-temperature surface, the vortex (marked with white particles) is penetrating into the flame zone, and (3) the thinned flame is shifted with the vortex significantly before being quenched.

A closer look at the flame structures in Figs. 4a to 4d suggests that up to $t = 11.1$ ms, the peak OH concentration and temperature decreased more at the axis of symmetry than at any other location in the flame zone as a result of the vortex-flame interaction. However, as the flame developed more

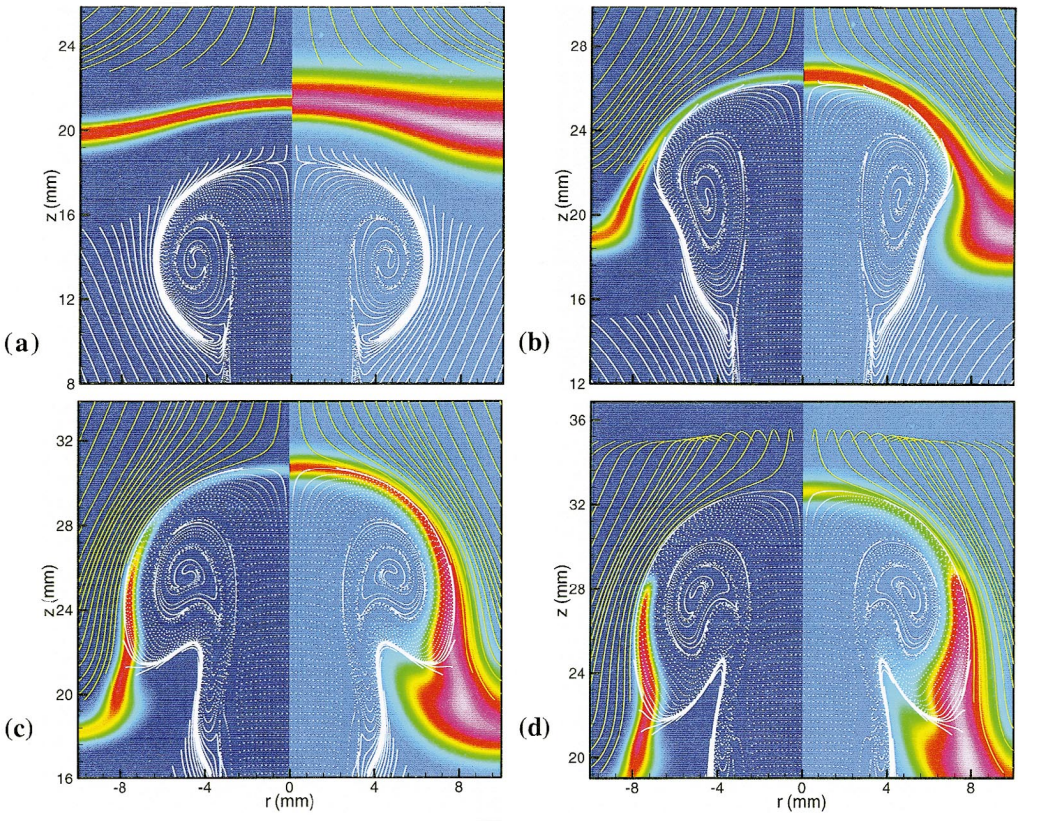

FIG. 4. Computed flames and flowfields obtained at instants (a) 9.1 ms, (b) 11.1 ms, (c) 12.1 ms, and (d) 12.54 ms. OH-concentration and temperature fields are shown on left and right halves, respectively. Instantaneous locations of particles that were injected from air and fuel nozzle are shown in white and yellow, respectively.

curvature for $t > 11.1$ ms, the lowest OH concentration and temperature locations shifted away from the axis. In Fig. 4c, the concentration of OH at $r = 5.3$ mm decreased below that of a stable flame (0.08%), whereas its concentration elsewhere is still above this level, suggesting that the flame is first quenched annularly at $r = 5.3$ mm. After another 0.44 ms of interaction (Fig. 4d), the flame is quenched in the region $r < 6$ mm. Interestingly, the combustion products are still present near the axis, while they are almost dissipated at $r = 5.3$ mm.

The computed flame in Fig. 4c qualitatively matches the OH image (Fig. 2) obtained during the experiments. In both flames, the diameter of the interacting vortex is the same (16 mm), and quenching is initiated at $r \sim 5.3$ mm. However, the computed flame appears to be pushed farther in the axial direction than the flame in the experiment. This difference could result from the flush-mounted syringe tube used in the model. The annular quenching process in the simulations is quantitatively shown in Fig. 5 by plotting the flame shape (broken line) and its temperature distribution (solid line) at different times during the vortex-flame-interaction process. The steady-state flame represented by line "a" is curved concave with respect to the fuel jet as a result of the difference in the densities and, hence, the velocities of the fuel and air jets. Nevertheless, the flame is at a uniform temperature of 1565 K (Line "1"). As the vortex pushes the flame toward the fuel jet, the flame temperature begins to decrease at the axis of symmetry. For $t > 11.1$ ms, the flame temperature is decreasing more in the region 4 mm $< r < 6$ mm than at the axis of symmetry. At $t = 12.1$ ms, the flame temperature of 1085 K at $r = 5$ mm is ~70 K lower than that at $r = 0$ mm and is ~45 K lower than that of the stable flame.

Time-accurate calculations using detailed chemistry and transport models can capture the annular-quenching pattern observed in the experiments. To further investigate the cause for annular quenching during the vortex-flame interaction, detailed flame

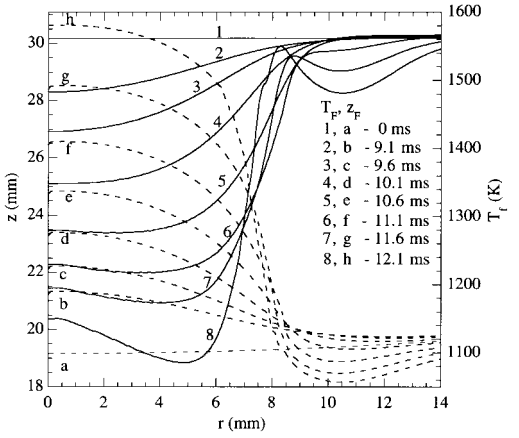

FIG. 5. Evolution of flame surface and changes in temperature during interaction with the vortex that originated on the air side.

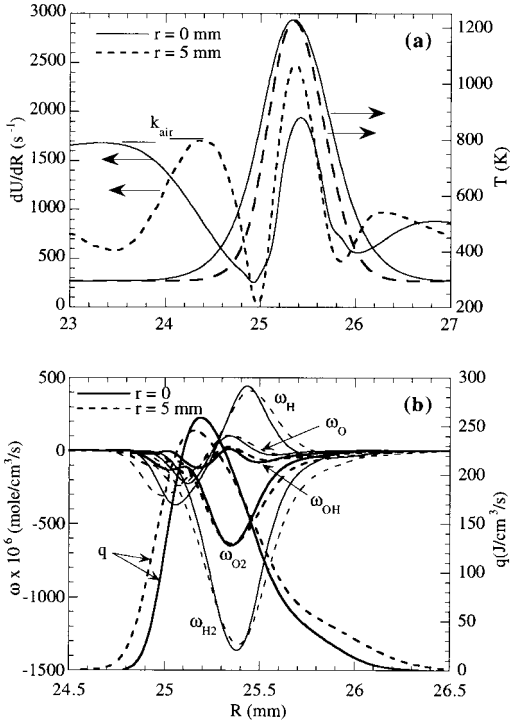

FIG. 6. Comparison of flame structure at the stagnation line with that located 5 mm away from the stagnation line obtained at $t = 11.1$ ms. (a) Velocity gradient and temperature variation normal to the flame surface and (b) variations in molar production and heat-release rates.

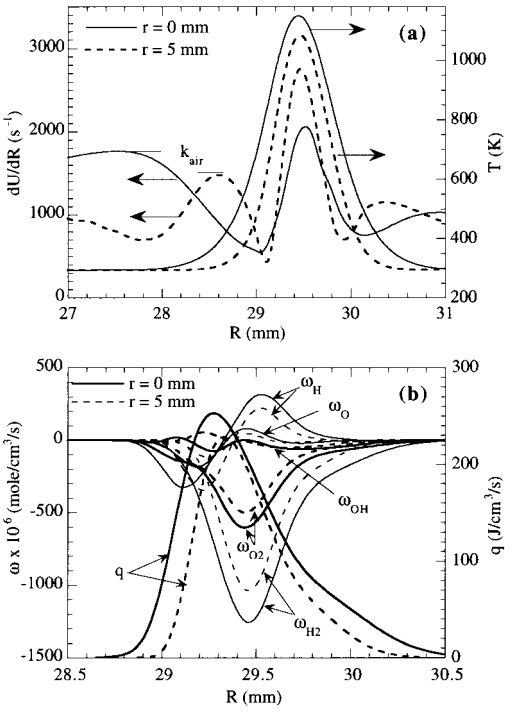

FIG. 7. Comparison of flame structure at the stagnation line with that located 5 mm away from the stagnation line obtained at $t = 12.1$ ms. (a) Velocity gradient and temperature variation normal to the flame surface and (b) variations in molar production and heat-release rates.

structures obtained from the data shown in Figs. 4b and 4c are plotted in Figs. 6 and 7, respectively. In each case the local flame structures obtained along the lines normal to the flame surface at $r = 0$ and 5 mm are compared. To gain a better understanding, the value of R (the distance in the direction normal to the flame) is adjusted to align the peak temperature locations.

Figure 6 suggests that the flame structures obtained at $r = 0$ and 5 mm are quite similar, except that the flame at 5 mm is slightly thicker. The flame at this instant is not extinguished at any radial location, and the flame temperature of 1228 K at $r = 0$ and 5 mm is greater than the quenching limit. Air-side strain rates calculated at both locations are nearly the same ($\sim$1700 s^{-1}), and are higher than the extinction limit (1410 s^{-1}) for the steady-state flame. It is known that unsteady flames can withstand to higher strain rates because of non-equilibrium-chemistry effects [6].

The flame temperature of 1085 K at $r = 5$ mm in Fig. 7 is below the quenching limit, whereas that at $r = 0$ mm is still above it. Interestingly, the strain rate (K_{air}) at $r = 5$ mm is lower than that at 0 mm, which suggests that the vortex-induced strain rate is

not totally responsible for the quenching at the former location. Close inspection of Fig. 5 reveals that the curvature (dz/dr) of the flame surface increases rapidly in the region 5 mm $>$ r $>$ 8 mm for times greater than 11.1 ms. In earlier studies of unsteady coflowing hydrogen jet diffusion flames [18,25], it was found that the temperature of the flame can increase or decrease as a result of the combination of preferential diffusion and curvature. Therefore, by use of the understanding gained in those studies and the analysis presented in this paper, the annular quenching observed during the vortex-flame interactions in opposing-flow hydrogen diffusion flames is thought to result from preferential diffusion and curvature—not strain rate.

Conclusion

Individual vortex-flame interactions are often studied to gain better understanding of turbulent-flame structures and, hence, to develop accurate turbulence-chemistry interaction models. A time-dependent CFDC code that incorporates 13 species and 74 reactions among the constituent species has been developed for the simulation of vortex-flame interactions in opposing-flow hydrogen jet diffusion flames. The model has been validated by directly simulating several steady-state axisymmetric counterflow diffusion flames and comparing the results obtained along the stagnation line with those computed with standard one-dimensional models and experiments.

Experiments were conducted to investigate the different quenching patterns one might expect during vortex-flame interactions in opposing-flow hydrogen jet diffusion flames. It was observed that when an air-side vortex is forced toward the flame at a relatively high speed, the flame at the stagnation line quenches, as expected, and the vortex passes through that hole. On the other hand, when the vortex is forced at a moderate speed, the flame surface deforms significantly and quenching develops in an annular manner away from the stagnation line. To investigate the processes involved in the development of such annular quenching, time-dependent calculations were performed for the opposing-flow jet flame using the axisymmetric CFDC code.

A steady-state opposing-flow jet flame was simulated first, and then a vortex was injected into the flow by ramping the velocity at the center portion of the air-jet exit to represent the syringe injection used in the experiment. Calculations performed with different injection times successfully captured the two extinction patterns (point and annular) observed in the experiments. Detailed analysis performed on the instantaneous data obtained just before the development of annular quenching and 1 ms later revealed that (1) the strain rate in the annular region is equal to or lower than that at the stagnation line, and (2) the flame curvature increases significantly in the annular region where the flame has began to quench. Based on the understanding gained from previous investigations of curvature effects in coaxial hydrogen jet flames and the findings of this study, it is thought that the unusual annular quenching observed during the vortex-flame interactions in opposing-jet diffusion flames is caused by the combined effect of preferential diffusion and flame curvature.

REFERENCES

1. Kee, R. J., Miller, J. A., Evans, G. H., and Dixon-Lewis, G., in *Twenty-Second Symposium (International) on Combustion,* The Combustion Institute, Pittsburgh, 1988, pp. 1479–1494.
2. Dixon-Lewis, G., in *Twenty-Third Symposium (International) on Combustion,* The Combustion Institute, Pittsburgh, 1990, pp. 305–324.
3. Chelliah, H. K., Law, C. K., Ueda, T., Smooke, M. D., and Williams, F. A., in *Twenty-Third Symposium (International) on Combustion,* The Combustion Institute, Pittsburgh, 1990, pp. 503–511.
4. Hottel, H. C., and Hawthorne, W. R., "Flame and Explosive Phenomena," in *Third Symposium (International) on Combustion,* The Combustion Institute, Pittsburgh, 1949, pp. 254–266.
5. Roquemore, W. M., Chen, L.-D., Goss, L. P., and Lynn, W. F., in *Turbulent Reactive Flows, Lecture Notes in Engineering* (R. Borghi and S. N. B. Murthy, eds.), Springer-Verlag, Berlin, 1989, Vol. 40, p. 49.
6. Darabiha, N., *Combust. Sci. Technol.,* 86:163 (1992).
7. Egolfopoulos, F. N. and C. S. Campbell, *J. Fluid Mech.,* 318:1 (1996).
8. Law, C. K., *Prog. Energy Combust. Sci.,* 10:295 (1984).
9. Mizomoto, M., Asaka, Y., Ikai, S., and Law, C. K., in *Twentieth Symposium (International) on Combustion,* The Combustion Institute, Pittsburgh, 1984, pp. 1933–1939.
10. Takagi T. and Xu, Z., *Combust. Flame* 96:50 (1994).
11. Roberts, W. L., Driscoll, J. F., Drake, M. C., and Ratcliffe, J. W., in *Twenty-Fourth Symposium (International) on Combustion,* The Combustion Institute, Pittsburgh, 1992, pp. 169–176.
12. Rolon, J. C., Aguerre, F., and Candel, S., *Combust. Flame* 100:422 (1995)
13. Ashurst, W. T., *Combust. Sci. Technol.* 92:87 (1993).
14. Poinsot, T., Trouve, A., Veynante, D., Candel, S., and Esposito, E., *J. Fluid Mech.* 177:265 (1987).
15. Rutland, C. J. and Ferziger, J. H., *Combust. Flame* 84:343 (1991).
16. Smooke, M. D., Ern, A., Tanoff, M. A., Valdati, B. A., Mohammed, R. K., Marran, D. F., and Long, M. B., in *Twenty-Sixth Symposium (International) on Combustion,* The Combustion Institute, Pittsburgh, 1996, p. 2161.

17. Katta, V. R. and Roquemore, W. M., *AIAA* paper 97-0904, Reno, Jan., 1997.
18. Katta, V. R., Goss, L. P., and Roquemore, W. M., *Combust. Flame* 96:60 (1994).
19. Frenklach, M., Wang, H., Goldenberg, M., Smith, G. P., Golden, D. M., Bowman, C. T., Hanson, R. K., Gardiner, W. C., and Lissianski, V., Gas Research Institute technical report GRI-95/0058, November 1, 1995.
20. Leonard, B. P., *Comput. Meth. Appl. Mech. Eng.* 19:59 (1979).
21. Katta, V. R., Goss, L. P., and Roquemore, W. M., *AIAA J.,* 32:84 (1994).
22. Sung, C. J., Liu, J. B., and Law, C. K., *Combust. Flame* 102:481 (1995).
23. Grisch, F., Attal-Tretout, B., Bouchardy, P., Katta, V. R., and Roquemore, W. M., *J. Nonlin. Opt. Phys. Mater.* 5:505 (1996)
24. Gutheil, E., Balakrishnan, G., and Williams, F. A., "Structure and Extinction of Hydrogen-Air Diffusion Flames," in *Lecture Notes in Physics* (N. Peters and B. Rogg, eds.), Springer-Verlag, New York, 1993, pp. 177–195.
25. Katta, V. R., and Roquemore, W. M., *Combust. Flame,* 100:61 (1995).

COMMENTS

Bernard Zamuner, French Aerospace Research Institute, (ONERA) France. Computational results of a steady laminar counter flow diffusion flame with a 1-D solver is often sensitive to the grid size. If your discretization is too rough, you may observe, for a particular stretch rate, extinction where the flame should survive. Did you perform grid dependence analyses in your 2-D computation?

Author's Reply. Numerical results, in general, are sensitive to the grid distribution. In the flame calculations, one might see extinction due to insufficient grid spacing, the exact grid spacing required to capture accurately the extinction process depends on the numerical schemes used. After performing calculations using different grid spacings, we found that 0.1-mm spacing in the axial and radial directions is sufficient to capture the extinction process that is independent of grid spacing.

•

Tadao Takeno, Nagoya University, Japan. Have you studied what is the appropriate parameter to predict the local extinction? We found the local dissipation rate can predict the occurrence of the local extinction [1].

REFERENCE

1. Yamashita, H., Shimada, M., and Takeno, T., in *Twenty-Sixth Symposium (International) on Combustion,* The Combustion Institute, Pittsburgh, 1996, pp. 27–34.

Author's Reply. We have not characterized the extinction conditions using local flow parameters. Although the local dissipation rate seems to predict extinction of a steady, nearly flat flame, it may not be sufficient to describe the extinction processes in a curved hydrogen flame. Some type of correction to the dissipation-rate vs. temperature relationship based on the local Lewis number and flame curvature is required.

•

H. N. Najm, Sandia National Laboratories, USA. The disappearance of OH radical is used in this work as an indicator of extinction. On the other hand, chemical production and consumption rates are available from this numerical simulation. In fact, the consumption rate of the fuel (H_2) was presented in the talk and was clearly nonzero in locations where OH disappeared. The results indicate little change (about 20% apparently) in H_2 consumption rate between flame regions where OH has disappeared and where it is still present. This suggests that the disappearance of OH in this flame is not an adequate indication of local extinction, at least as far as the model and chemical mechanism used in this work are concerned.

Author's Reply. Extinction represents a process in which the chemical kinetics transform from flame to no-flame reactions. Extinction does not occur instantaneously; rather, it occurs over a period of time (typically in several hundred μs). OH concentration, heat release rate, or any other quantity represents only a particular state in this extinction process. It is obvious that the first sign of the disappearance of the OH radical does not represent an extinguished flame; nevertheless, it does indicate a well-advanced state in the extinction process. The temperature and H_2 consumption rate in Fig. 7 suggest that the flame in region $r = 5$ mm is going through the extinction process, while stable burning is taking place in the region $r = 0$ mm. Figures 4c and 4d show that changes in temperature are evident only 440 μs after the changes in OH are observed. In the simple diffusion flames investigated in this paper, disappearance of the OH radical always leads to complete extinction in a few microseconds. On the other hand, in certain premixed flames, the extinction process may be terminated after the disappearance of the OH radical—in those situations, tagging the OH radial to extinction is not sufficient.